ChemPubSoc Europe

DOI: 10.1002/cphc.201701024

CHEMPHYSCHEM Articles

Special Issue

A Systematic Study of Isomorphically Substituted H-MAlPO-5 Materials for the Methanol-to-Hydrocarbons Reaction

Magnus Mortén,[a] Łukasz Mentel,[a] Andrea Lazzarini,[a] Ilia A. Pankin,[b, c] Carlo Lamberti,[b, c] Silvia Bordiga,[b] Valentina Crocellà,[b] Stian Svelle,[a] Karl Petter Lillerud,[a] and Unni Olsbye*[a]

Substituting metals for either aluminum or phosphorus in crystalline, microporous aluminophosphates creates Brønsted acid sites, which are well known to catalyze several key reactions, including the methanol to hydrocarbons (MTH) reaction. In this work, we synthesized a series of metal-substituted aluminophosphates with AFI topology that differed primarily in their acid strength and that spanned a predicted range from high Brønsted acidity (H-MgAlPO-5, H-CoAlPO-5, and H-ZnAlPO-5) to medium acidity (H-SAPO-5) and low acidity (H-TiAlPO-5 and H-ZrAlPO-5). The synthesis was aimed to produce materials with homogenous properties (e.g. morphology, crystallite size, acid-site density, and surface area) to isolate the influence of metal substitution. This was verified by extensive characterization. The materials were tested in the MTH reaction at 450 °C by using dimethyl ether (DME) as feed. A clear activity difference was found, for which the predicted stronger acids converted DME significantly faster than the medium and weak Brønsted acidic materials. Furthermore, the stronger Brønsted acids (Mg, Co and Zn) produced more light alkenes than the weaker acids. The weaker acids, especially H-SAPO-5, produced more aromatics and alkanes, which indicates that the relative rates of competing reactions change upon decreasing the acid strength.

1. Introduction

Controlled synthesis of advanced, functional materials at the nanoscale is now becoming achievable. However, decoupling individual material properties and assessing their influence on material functionality remains a challenge.

For zeolites and zeotypes, a class of microporous aluminosilicates and aluminophosphates, control over material properties is already quite advanced. Extended research efforts devoted to finding procedures driving the synthesis towards materials with desired properties have resulted in methodologies that allow control over particle size and morphology,[1–4] incorporation and distribution of active sites,[5,6] and the construction of new topologies.[7] Moreover, the efforts are further stimulated by novel applications emerging to exploit the advanced material properties.[8,9]

The quest for linking structure and material properties to activity, "the materials genome", is ongoing, with the main challenge of identifying the key properties of the materials.[10] By understanding and quantifying structure–activity relationships, a more rational approach to catalyst design is possible, improving existing and developing new processes. In surface science, considerable effort has been made to establish a descriptor-based approach to transition-metal catalysis, linking measurable properties of the catalyst structure with activity and selectivity in catalyzed reactions.[11,12] Control of material properties is thus of key importance in this quest, as it makes it possible to investigate the influence of the individual factors on the performance of the materials. The understanding gained from those investigations could subsequently be used to optimize the performance of the materials for selected applications.

A particularly challenging process is the methanol-to-hydrocarbons reaction (MTH), in which methanol or dimethyl ether (DME) is converted into larger hydrocarbons over a Brønsted acidic zeotype catalyst. Numerous studies have aimed to reveal how each of the material properties (e.g. catalyst composition, topology, morphology, crystal size, and density of

[a] M. Mortén, Ł. Mentel, A. Lazzarini, S. Svelle, K. P. Lillerud, Prof. U. Olsbye
Centre for Materials Science and Nanotechnology
Department of Chemistry, University of Oslo
P.O. Box 1033, Blindern, 0315 Oslo (Norway)
E-mail: unni.olsbye@kjemi.uio.no

[b] I. A. Pankin, C. Lamberti, S. Bordiga, V. Crocellà
Department of Chemistry, CrisDi Interdepartmental Centre and INSRM reference, University of Turin
via Pietro Giuria 7, 10125 Turin (Italy)

[c] I. A. Pankin, C. Lamberti
International Research Center "Smart Materials"
Southern Federal University, Zorge Street 5
344090 Rostov-on-Don (Russia)

Supporting Information and the ORCID identification number(s) for the author(s) of this article can be found under: https://doi.org/10.1002/cphc.201701024.

An invited contribution to a Special Issue on Reactions in Confined Spaces

acid sites) can be optimized to improve conversion capacity, activity, and product selectivity.[13,14]

The mechanism of MTH has been debated extensively with more than 20 unique mechanisms proposed to explain the initial carbon–carbon bond-formation process.[13] However, under steady-state conditions Dahl and Kolboe have proposed that reactions occur through a hydrocarbon pool mechanism, by which sequential methylation and elimination reactions occur on adsorbed carbon species at the active site of the catalyst, co-catalyzing product formation.[15–17] Alkenes and aromatics constitute important adsorbed pool species promoting the two distinct product-forming cycles (Scheme 1).

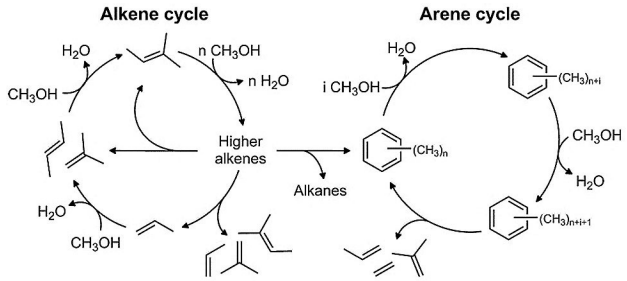

Scheme 1. General reaction scheme for the dual-cycle mechanism. Figure from ref. [18].

In the alkene cycle, alkenes undergo methylation and cracking reactions typically to give C_3 to C_5 alkenes as major products.[19] In the arene cycle, aromatics are methylated to substituted aromatics and undergo elimination reactions to form light alkenes and aromatics with fewer substituents as products.[19b,20] This latter reaction links the arene and alkene cycles. Another main reaction linking the two cycles is hydrogen transfer from either methanol or DME to an adjacent alkene, followed by addition of the dehydrogenated species to another alkene molecule, which leads to diene formation. Subsequent cyclization and hydrogen-transfer reactions finally lead to the formation of aromatic products.[21–23]

The active site of the MTH reaction is a Brønsted acid site (BAS). Although the fundamental aspects of solid Brønsted acidity are still under active investigation, there is extensive literature covering experimental and computational approaches for the construction of relative acid strength scales.[24,25] Numerous approaches to quantify acidity have been suggested by using probe molecules, usually basic, in combination with an experimental probe detection technique. Examples include NH_3, CO, alcohols, nitriles, and aromatic molecules and common probe detection methods such as infrared spectroscopy, NMR spectroscopy, and temperature-programmed desorption with mass spectrometry.[24,25] A computational alternative is the deprotonation energy (DPE)[26,27] and NH_3 adsorption enthalpy,[28,29] which allow quantifiable ranking of acidity.

A few recent studies have addressed the influence of BAS strength on the MTH reaction. By using infrared spectroscopy and CO as a probe, the acidity difference of two isostructural zeolite/zeotype materials, H-SSZ-24 and H-SAPO-5, was established.[18,30] The more acidic zeolite H-SSZ-24 produced more aromatics and C_2–C_3 hydrocarbons upon feeding MeOH, whereas more weakly acidic H-SAPO-5 showed increased selectivity towards C_4–C_{6+} alkenes. It was concluded that the differences in product selectivity could be ascribed to the arene cycle being promoted over the more acidic material, whereas the alkene cycle was favored for the weaker acid.[30] More recently, a study in which methanol and DME were compared as MTH feedstock provided additional insight into the matter. Importantly, it was found that methanol promoted hydrogen-transfer reactions to a much higher extent than DME. Hence, the DME/methanol ratio in the reactor had substantial influence on product selectivity and catalyst conversion capacity. Furthermore, the study showed that the reversible methanol condensation reaction to DME and water was equilibrated over H-SAPO-5 but not over H-SSZ-24 under the MTH reaction conditions.[31] This study showed that the difference in product selectivity observed for H-SSZ-24 and H-SAPO-5 could at least partly be ascribed to their different activities for the methanol condensation reaction relative to subsequent methylation reactions.

The effect of BAS strength on a key MTH reaction step, olefin methylation, was explored computationally by Brogaard and Wang et al.[28,29,32] Ammonia adsorption enthalpy was identified as a descriptor for BAS strength over a series of metal-substituted aluminophosphates, ranking the materials on the basis of the BAS strength of the site created by isomorphic substitution. A scaling relationship for methylation rates of ethene and propene and BAS strength was established for several topologies and material compositions, yielding a predictive relationship for turnover frequencies of propene methylation on the basis of the ammonia adsorption enthalpy on the BAS.

One of the investigated topologies, AFI, with unidimensional 12-ring channels (7.3 Å × 7.3 Å), is ideal for experimental verification, as it allows for bulky molecules to diffuse out of the structure, thereby limiting secondary reactions. In addition, since the discovery of AlPO-5 in 1982 by Wilson et al.,[33] numerous examples of compositional variants substituting heteroatoms in the structure have been reported, including the elements Mg, Zn, Co, Ti, Zr, and Si.[5,34] It has been debated whether isomorphic substitution of metals for either Al or P in the AFI structure, thereby creating a Brønsted acid site, is even possible.[35] However, several elements have been subject to rigorous study by employing advanced spectroscopic techniques, which have confirmed framework incorporation.[36] Metal-substituted AlPO-5 materials have been tested as catalysts in several reactions, including methanol to hydrocarbons,[37] ethylation and propylation of aromatics,[38,39] cracking of alkanes,[40] and aromatic isomerization.[41]

In this work, we aim to study the effect of metal incorporation into the AlPO-5 structure and the effect of the created BAS on the MTH reaction. This will be a single-parameter study attempted by synthesizing a series of metal-substituted AlPO-5 materials with the same topology, similar crystal size, same morphology, and same BAS density. The materials were extensively characterized to ensure that the catalyst lattices, includ-

ing the immediate surroundings of the heteroatoms, were intact during testing. Furthermore, to avoid the influence of feed composition, DME was used as MTH feedstock instead of MeOH, keeping the DME/MeOH/H_2O ratio in the reactor similar across the materials. To the best of our knowledge, this is the first detailed, systematic study of metal-substituted ALPO-5 materials used in the MTH reaction.

2. Results and Discussion

2.1. Synthesis and Catalyst Characterization

A summary of the obtained characterization data, including the size of the particles [from scanning electron microscopy (SEM) images], specific surface area (from BET), acid-site density estimated from *n*-propylamine temperature-programmed desorption (TPD), and the heteroatom content obtained on the basis of energy-dispersive X-ray spectroscopy (EDS) measurements, for all of the synthesized materials can be found in Table 1.

Table 1. Key material characteristics for the synthesized H-MAlPO-5 materials.

Material	Crystal size [μm]	SA_{BET}[a] [$m^2 g^{-1}$]	Acid-site density[b] [mmol g^{-1}]	Density of M[c] [mmol g^{-1}]
H-MgAlPO-5	1×2.5	360	0.102	0.1
H-ZnAlPO-5	1×2.5	362	0.094	0.2
H-CoAlPO-5	1.5×2	347	0.081	0.2
H-SAPO-5[d]	1×2	340	0.068	0.3
H-ZrAlPO-5	2×4.5	352	0.065	–[e]
H-TiAlPO-5	3.5×3	329	0.060	0.2
AlPO-5	1×1	370	–	–[f]

[a] BET surface area. [b] Determined by *n*-propylamine TPD. [c] Estimated from EDS on the basis of the ratio of M and either Al or P. [d] See ref. [42]. [e] Overlap between Zr/P peaks; no estimate obtained. [f] No heteroatom detected by EDS.

The X-ray diffractograms were measured for the as-synthesized (Supporting Information, Section S1) and calcined materials (Figure 1). All materials were highly crystalline and showed the AFI structure as the only phase present. The materials were stable up to 550 °C during calcination and showed no sign of degradation after heating, as is evident from the X-ray diffraction (XRD) patterns of the calcined samples (Figure 1).

The BET areas of the samples were determined to fall between 329 and 362 $m^2 g^{-1}$, with H-TiAlPO-5 and H-ZnAlPO-5 being the two extremes of the metal-substituted series. Non-substituted AlPO-5 showed a slightly higher surface area of 370 $m^2 g^{-1}$ (Table 1). These results indicate that little pore blocking due to extra framework metal species occurs.

Representative SEM images (Figure 2) show the hexagonal barrel-shaped morphology of the samples. The crystallites have a homogenous size distribution with typical averages between 1 and 2 μm in diameter and 2 and 3 μm along the *c* axis. H-ZrAlPO-5 and H-TiAlPO-5 show slightly larger crystallites, with

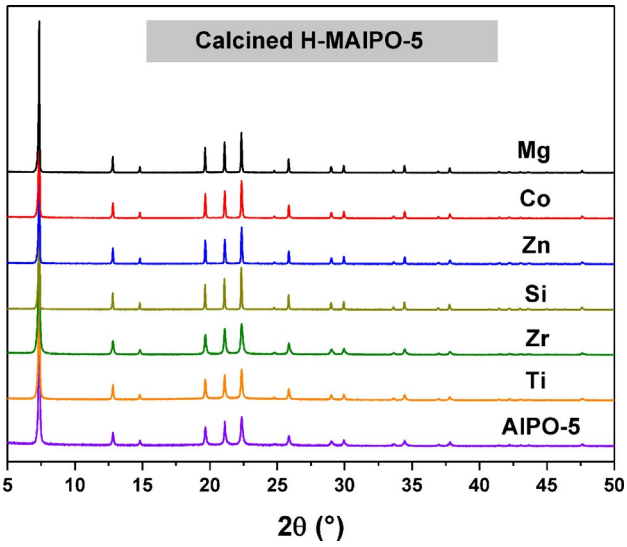

Figure 1. XRD powder patterns of the calcined H-MAlPO-5 materials and AlPO-5 used in this work (see Section S1 for the XRD powder patterns for the as-synthesized samples).

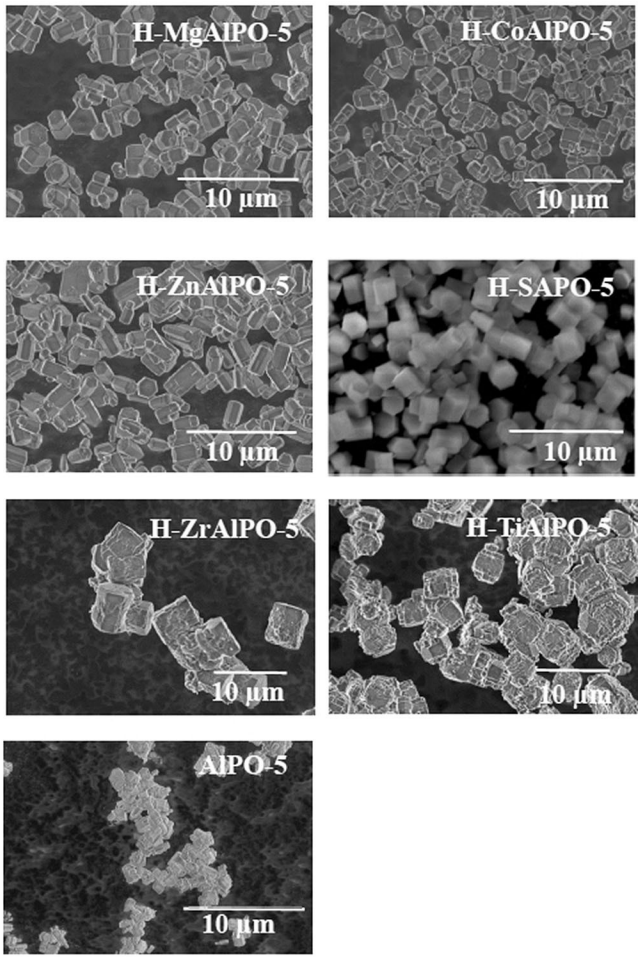

Figure 2. SEM images of the H-MAlPO-5 materials and AlPO-5.

averages from 2 to 4 μm in diameter and 3 to 5 μm along the *c* axis. The morphology of both samples resembles hexagonal

barrels, but with edges that are less well defined than those of the rest of the synthesized materials.

n-Propylamine TPD was used to probe the Brønsted acidity and to quantify the density of the Brønsted acid sites. The desired density of the Brønsted acid sites was 0.1 mmol g^{-1}, a value that was previously reported for most of the materials synthesized in this work.[37,43] Table 1 shows that the density of acid sites varies somewhat between the +2 and +4 metals. The density of acid sites is lower for the +4 metals than for the +2 metals, ranging from 0.060 to 0.065 and 0.068 mmol g^{-1} for H-TiAlPO-5, H-ZrAlPO-5, and H-SAPO-5, respectively. This is in agreement with the +4 metals being less likely to substitute into the framework, as P–O bonds are more covalent in character than Al–O bonds in the ALPO-5 framework.[44] For the +2 metals, the density of acid sites varies from 0.081 to 0.094 and 0.102 mmol g^{-1} for H-CoAlPO-5, H-ZnAlPO-5, and H-MgAlPO-5, respectively. To investigate the effect of varying the acid-site density on the MTH reaction, experiments with a higher density sample (Mg) and lower density sample (Zn) were performed (Section S2). The product selectivities do not vary significantly between the high- and low-density samples under these conditions, so it is concluded that the variation in the acid-site density between the samples is satisfactory for the present study.

The estimates of metal content from EDS provide complementary information to the density of Brønsted acid sites obtained from *n*-propylamine TPD, from which we can infer the amount of metal present in the sample that is not incorporated into the lattice as BAS. As can be seen in Table 1, the total density of metals varies somewhat between the samples, ranging from 0.1 to 0.2 mmol g^{-1} for the materials synthesized in this work. Rough agreement between the samples is expected, as the same synthetic procedure was followed, adding the same amount of metal salts to the synthesis gel. The excess amount of metal can exist as a variety of species that are hard to identify precisely; however, except for the H-SAPO-5 sample, the amounts of those species are small.

Direct evidence of metal incorporation into the AlPO-5 framework and the consequent formation of strong Brønsted acid sites were assessed through IR spectroscopy. Due to the prohibitive particle dimensions in transmission measurements, the samples were studied in reflectance mode (see the Experimental Section). Figure 3 shows the spectra collected after sample activation at 450 °C under helium flow for the full set of samples.

As already described, the IR spectra of the H-MAlPO-5 materials (AFI topology) are characterized by strong bands in the region below $\tilde{\nu}$ = 2500 cm^{-1}, which are assigned to overtone and combination vibrations of the lattice. Above $\tilde{\nu}$ = 2500 cm^{-1}, absorption bands attributed to the stretching vibrations of the hydroxy groups are observed.[45] In all spectra, a characteristic band at $\tilde{\nu}$ = 3674 cm^{-1} ascribed to the terminal P–OH groups is present. Moreover, in H-SAPO-5 and AlPO-5 the respective bands for the Si–OH and Al–OH terminal groups are present at $\tilde{\nu}$ = 3790 and 3735 cm^{-1}. The only sample that shows well-defined maxima ascribable to bridging Brønsted sites is H-SAPO-5 ($\tilde{\nu}$ = 3625 cm^{-1}), whereas other H-

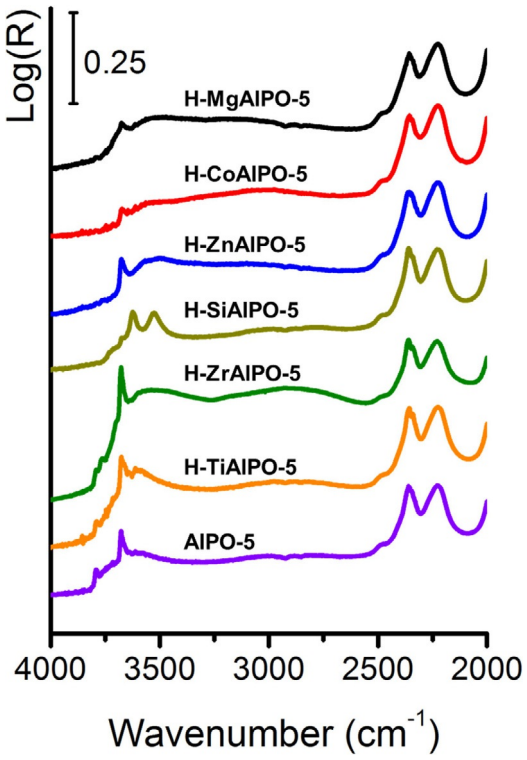

Figure 3. DRIFT spectra of AlPO-5 and H-MAlPO-5 after activation at 450 °C under a He atmosphere. The spectra were collected at 120 °C to avoid moisture contamination and water adsorption.

MAlPO-5 materials are characterized by a continuum in the spectra profile, which suggests that the OH group is engaged in hydrogen bonding.[37] All of these OH species in the spectral region below $\tilde{\nu}$ = 3650 cm^{-1} are usually ascribed to OH bonds presenting Brønsted acidity, as reported in the literature for these materials.[46]

To investigate the nature of the acid sites in more detail, selected samples (i.e. Mg, Co, Si, and pure AlPO-5) were studied by using CD_3CN as a probe molecule (see Section S3). All of the samples analyzed exhibit the following spectral features: 1) a broad band centered at $\tilde{\nu}$ = 2310–2315 cm^{-1}, ascribed to the probe adsorbed on Al^{3+} Lewis acid sites; 2) a sharp band at $\tilde{\nu}$ = 2263 cm^{-1}, due to physisorbed CD_3CN; 3) a band between $\tilde{\nu}$ = 2285 and 2275 cm^{-1}, assigned to the probe adsorbed on terminal (phosphanols) and bridged hydroxy groups (Brønsted sites); 4) samples including Co^{2+} and Mg^{2+} also show a feature (well visible in the last desorption step; gray spectra in the insets) centered at $\tilde{\nu}$ = 2301–2304 cm^{-1}, assigned to acetonitrile adsorbed on Lewis sites created by the incorporated M^{2+} cations.[46,47] These observations are in line with older literature, which showed that the AlPO-5 framework was so flexible that Al could interact with strong basic probes as a Lewis acid without losing its tetrahedral lattice coordination.[48] The complexity of the IR spectra further suggests that ranking of Brønsted acid strength for these materials must rely on theoretical predictions.

To sum up, the characterization data presented in this section show that the materials form a series with similar key

properties such as particle size, morphology, surface area, and acid-site density. The materials differ in one respect, namely, the nature of the isomorphically substituted heteroatom. This makes the series of materials well suited for a one-parameter variation study, in which the catalytic properties of the created Brønsted acid sites can be ascribed to differences in acid strength.

2.2. Catalytic Testing

2.2.1. Catalytic Activity of H-MAlPO-5 Materials at 450 °C in the MTH Reaction

Although metal-substituted aluminophosphates have been studied extensively for over 30 years, there are only a few systematic studies in which a consistent series of materials was examined to uncover the dependence of catalytic properties on the substituted element forming the BAS. In pioneering studies on H-MAlPO-5 materials with M = Mg, Co, Zn, Si, and Zr were tested for MeOH conversion at 370 °C.[37] Lischke et al. found that H-SAPO-5 was the most-active catalyst, followed by H-CoAlPO-5. H-MgAlPO-5 and H-ZnAlPO-5 were found to be significantly less active, and H-ZrAlPO-5 showed negligible conversion. In an analogous study of H-SAPO-5 and H-CoAlPO-5, Popova et al. reported that the initial conversion of MeOH was similar over H-CoAlPO-5 and H-SAPO-5 at 450 °C.[49]

In the present contribution, the Brønsted acidic H-MAlPO-5 materials were designed to span a spectrum of acid strengths covering the high, medium, and low values[32] while keeping properties such as particle size and morphology and density of acid sites maximally similar to a degree allowed by the synthetic procedure. The choice of the substituting elements was strongly influenced by the work of Brogaard and Wang et al., who used ammonia adsorption enthalpy as an acidity descriptor; they established a ranking of the materials that correlated with rates of propene methylation.[28,29]

All synthesized H-MAlPO-5 materials were tested as catalysts in the MTH reaction to evaluate catalytic activity. The MTH reaction is catalyzed by Brønsted acid sites and thus serves both as an indirect means of confirming framework incorporation of metals by demonstrating activity[35] and as a probe for the influence of the strength of the created BAS through the activities and selectivities across the materials. The H-MAlPO-5 materials were tested at 450 °C and low feed rates (weight hourly space velocity, WHSV = 1.9 h^{-1}) and a low DME partial pressure (13 mbar, 1 mbar = 0.1 kPa) to ensure catalytic activity across the series. Table 2 summarizes the activity of the catalysts expressed as initial turnover frequency (TOF) and initial conversion rate per gram of catalyst (r_{conv}). The theoretically calculated value for ammonia adsorption energy is included in the table as an acid-strength descriptor and serves as a theoretical ranking of the materials from strong to weak Brønsted acids. This ranking will be used throughout the discussion upon addressing acid strength.

Before proceeding to the test results, it should be noted that the DME-to-methanol ratio versus conversion graphs in the reactor effluent overlap for all tested materials (Section S4), which demonstrates that the activity and selectivity differences observed between the materials are not related to the relative abundances of DME, methanol, and water in the reactor.

Table 2. H-MAlPO-5 theoretical acid strength (ΔE_{NH_3}; given in kJ mol^{-1}), turnover frequency (TOF; values in $mol_{prod}\,mol_{[H^+]}^{-1}\,h^{-1}$), and rate of DME conversion (r_{conv}; values in $10^{-2}\,mol_{prod}\,g_{cat}^{-1}\,h^{-1}$).[a]

Material	ΔE_{NH_3} [b]	TOF	r_{conv}
H-MgAlPO-5	−128	243	2.48
H-CoAlPO-5	−121	279	2.27
H-ZnAlPO-5	−119	217	2.04
H-SAPO-5	−83	118	0.80
H-ZrAlPO-5	−75	30	0.20
H-TiAlPO-5	−75	39	0.24
AlPO-5	–	–	0.13

[a] Conditions: 450 °C, p_{DME} = 13 mbar, WHSV = 1.9 h^{-1}. [b] See Section S6.

As can be seen in Table 2, the three most-active catalysts are H-MgAlPO-5, H-CoAlPO-5, and H-ZnAlPO-5 with initial TOF values of 243, 279, and 217 $mol_{prod}\,mol_{[H^+]}^{-1}\,h^{-1}$, respectively. H-SAPO-5 gives an initial TOF of 118 $mol_{prod}\,mol_{[H^+]}^{-1}\,h^{-1}$, a value that is twofold smaller than the TOFs of the three strongest acids, whereas H-ZrAlPO-5 and H-TiAlPO-5 give TOF values of 30 and 39 $mol_{prod}\,mol_{[H^+]}^{-1}\,h^{-1}$, respectively. The activity of the catalysts corresponds well with the theoretical acidity ranking based on ammonia adsorption energy. This trend is in line with the scaling relation developed by Brogaard and Wang et al. between NH_3 adsorption enthalpy and alkene methylation rate over H-MAlPO-5 materials.[32] Furthermore, previous mechanistic studies point to a reaction between sorbed species as the rate-determining step of both hydrogen-transfer reactions (leading to the first C–C bond formation; i.e. to initiation of the MTH reaction) and alkene/arene methylation reactions (the propagation reactions of the dual-cycle MTH mechanism).[31,50,51] The rate of such reactions generally increases upon increasing the coverage of the active site, which is, in this case, induced by a higher acid strength. The catalysts can be grouped on the basis of both their performance, measured by the theoretical acidity, and initial TOF/r_{conv}, as high acidity/activity (Mg, Co, Zn), medium acidity/activity (Si), and low acidity/activity (Zr/Ti). This grouping coincides well with a grouping that can be made on the basis of the chemical nature of the doping element. Mg, Co, and Zn are formally +2 and are incorporated in place of Al atoms; Zr and Ti both have +4 oxidation state and substitute P lattice position, the same as Si. However, Si is the only metalloid in the +4 series, and it is the most similar to P in size, which suggests that it will exert the smallest perturbation on the framework compared to Zr and Ti, which are transition metals and have larger ionic radii. The different behavior of the +2 and +4 sites can be further rationalized in view of the findings presented by Corà and Catlow, who showed that AlPOs exhibited molecular-ionic character that was a consequence of being composed of Al^{3+} and PO_4^{3-} ions.[44]

Unsubstituted AlPO-5 is also included in the series. Given that it does not contain any M–(OH)–P/Al bridge sites, it can serve as a benchmark for the low-activity samples. Under the

studied conditions, AlPO-5 showed conversion of DME into hydrocarbons, however, at a lower rate than H-ZrAlPO-5 and H-TiAlPO-5 (0.13 vs. 0.20 and 0.24×10^{-2} $mol_{prod}\,g_{cat}^{-1}\,h^{-1}$). The conversion of DME over AlPO-5 may be ascribed to weakly acidic P–OH-groups. The P–OH groups can catalyze the dehydration of methanol to DME and at higher temperatures convert MeOH and DME into hydrocarbons.[52] To investigate the difference in the activities of H-ZrAlPO-5 and AlPO-5, a series of experiments were performed on the two materials and a physical mixture of ZrO and AlPO-5 (Section S7). The activity and product selectivity of H-ZrAlPO-5 is substantially different from those of AlPO-5 and the ZrO/AlPO-5 physical mixture. The significant difference in activities between AlPO-5 and either H-ZrAlPO-5 or H-TiAlPO-5 indicates that isomorphic substitution of Zr or Ti into the AlPO-5 framework creates a Brønsted acid bridge site that alters the materials' catalytic properties. Overall, the MTH results show that the materials in this series have BAS with significant activity differences, and this corresponds well with theoretical predictions of Brønsted acid strength.

2.2.2. Product Selectivity

To investigate the influence of the different isomorphic substitutions into the AlPO-5 framework on product selectivity during the MTH reaction, the synthesized H-MAlPO-5 materials were tested at 450 °C with variable feed rates (WHSV = 0.23–1.9 h^{-1}) to obtain comparable initial conversion levels. By reducing the feed rate, an initial conversion level of about 80% is obtained for H-MgAlPO-5, H-CoAlPO-5, H-ZnAlPO-5, and H-SAPO-5. For H-ZrAlPO-5 and H-TiAlPO-5, the highest conversion levels obtained are 30 and 12%, respectively, by employing very-low feed rates (see the Experimental Section). Previous studies of the MTH reaction showed that conversion–selectivity trends were often linear between 15 and 85% conversion but differed widely for higher and lower conversion.[53] This is indeed what we observe for all materials except for H-TiAlPO-5, for which the conversion does not rise above 12%, and therefore, the H-TiAlPO-5 sample will not be included in the remainder of the discussion.

The conversion–selectivity results reported in Figures 4–8 were obtained during deactivation of the samples. This procedure was warranted by previous studies of H-SAPO-5 as a MTH catalyst. It was shown that the conversion–selectivity graphs overlapped for fresh versus deactivated samples.[42] Additional tests performed in the present study over H-MgAlPO-5 at two different space velocities led to the same conclusion (Section S8).

The selectivity to three main categories of products, namely, alkenes, alkanes, and aromatics, was chosen to illustrate the principal trends and to highlight selectivity variations with heteroatom substitution (see Section S5 for the full set of selectivities).

Light alkenes, and propene in particular, are currently the target products of the majority of industrial MTH plants.[53] Figure 4a shows that the selectivity to alkenes for Mg, Co, Zn, and Si is approximately constant, at a very high level (70–90%), between 15 and 85% conversion, whereas for Zr it steadily increases towards 40% with increasing conversion. The most striking feature of alkene selectivity is the distinct behavior exhibited by material groups categorized according to the predicted acid strength. The stronger Brønsted acidic materials (Mg, Co and Zn) give significantly higher alkene selectivity than medium acidic H-SAPO-5. Weakly acidic H-ZrAlPO-5 gives the lowest alkene selectivity of the tested materials.

Moving on to selectivity to alkanes and aromatics (Figure 4b,c), their selectivity trends are generally opposite to those of the alkenes. Their selectivity decreases from the weakest Brønsted acid, H-ZrAlPO-5, to the strongest acid, H-MgAlPO-5, and H-CoAlPO-5 lies slightly outside the general trend for alkanes (see below). In the MTH reaction scheme, alkanes and aromatics are typical products originating from hydrogen-transfer reactions.[13,20] The results presented in Figure 4 suggest that isomorphic substitution of a metal into the aluminophosphate structure significantly alters the chemistry associated with the created Brønsted acid sites, shifting the product spectrum towards alkenes for the more acidic materials.

Turning next to individual alkenes, ethene, propene, and C_{5+} selectivity versus conversion for each material is shown in Figure 5. A striking observation in Figure 5a is the systematic increase in propene selectivity with increasing catalyst acid strength. At 75% conversion, the selectivity to propene spans a gap from 25 C% for H-SAPO-5 to almost 50 C% for H-MgAlPO-5. The difference in propene selectivity is also significant at lower conversion levels, ranging from 30 C% over H-MgAlPO-5, via 15 C% over H-SAPO-5, to 10 C% over H-ZrAlPO-5, all at 20% conversion. Another evident feature of the propene selectivity plot is the rapid increase in propene selectivity with increasing conversion. The slope of the curve is similar to that for the Mg-, Co-, and Zn-containing materials and is somewhat lower than that for the Si- and Zr-containing materials. An opposite trend is observed for the C_{5+} alkenes (Figure 5b): their selectivity decreases with increasing acid strength and with increasing conversion; the slope is steep and negative for the Mg-, Co-, and Zn-containing materials; slightly negative for H-SAPO-5; and positive for H-ZrAlPO-5.

Alkenes are intermediate, autocatalytic species in the MTH reaction. Reactions leading to their formation and conversion include the methylation, oligomerization, and cracking of short- and long-chain alkenes, as well as dealkylation of aromatic compounds, in particular polymethylated benzene molecules.[13,20,30,54,55] The results presented in Figure 5 suggest that a high acid strength favors cracking of higher alkenes to form propene. This conclusion is in line with literature reports, which showed that only strongly acidic zeolites could crack C_{5+} alkenes to light C_2 and C_3 alkenes, whereas less-acidic zeotypes favored oligomerization followed by cracking to higher alkenes.[56,57] Interestingly, Miyaji et al. showed that 2-methyl-2-butene and 1-pentene were not cracked in a monomolecular mechanism over H-SAPO-5,[75] in line with the results presented in Figure 5. Furthermore, Meusinger et al. studied cracking of *n*-hexane and *n*-butane over H-MgAlPO-5, H-CoAlPO-5, and H-SAPO-5.[58] These authors observed that comparable samples

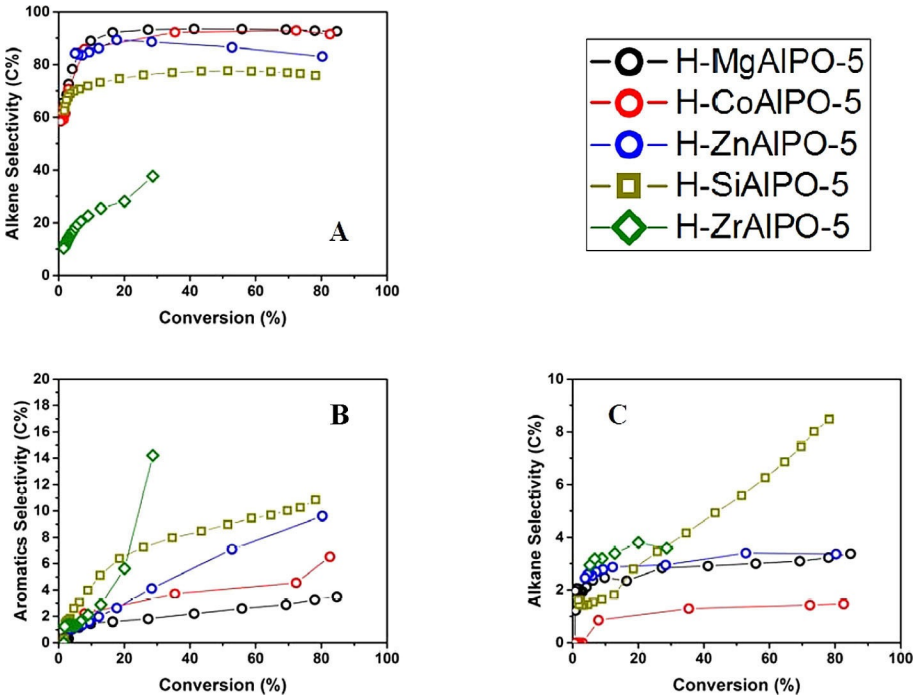

Figure 4. Product selectivity for DME conversion into three major product categories at 450 °C over the H-MAlPO-5 materials. Alkenes include ethene, propene, butenes, pentenes, and identified C_{6+} alkenes.

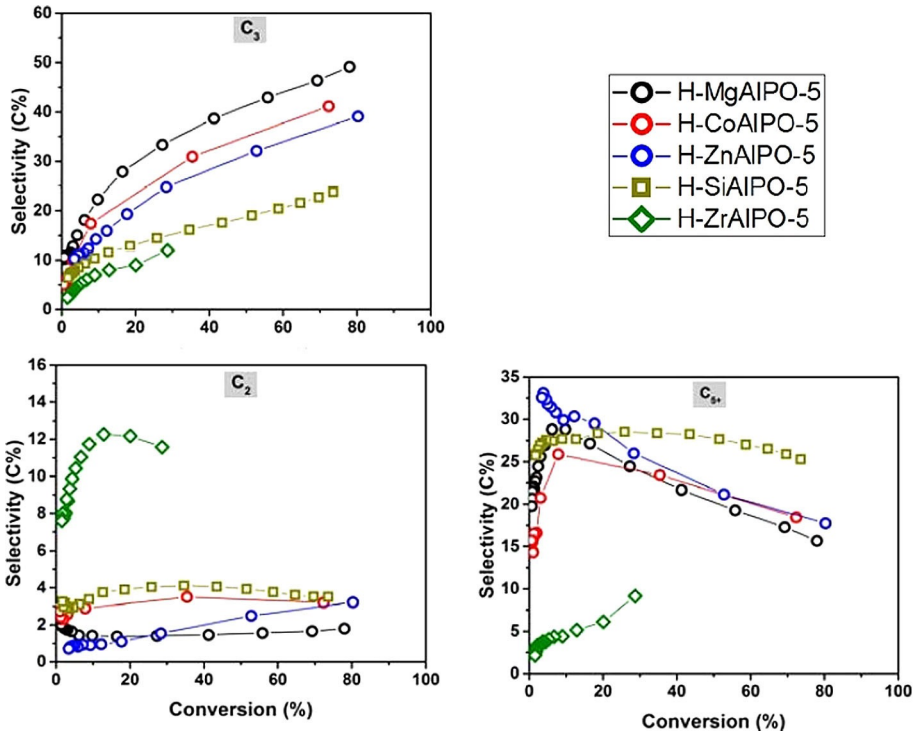

Figure 5. Product selectivity for DME conversion into C_3, C_2, and C_{5+} at 450 °C over the H-MAlPO-5 materials.

of the materials (acid-site density, crystal size) gave a ranking based on the TOF as H-MgAlPO-5 > H-CoAlPO-5 > H-SAPO-5. A comparison between the ethene and propene selectivity plots (Figure 5 a, c) shows that the two products have opposite trends with respect to selectivity versus predicted catalyst acid strength. This result suggests that the two products are formed by mechanistically distinct routes. Ethene formation was previously assigned to polymethyl benzene dealkylation,[13, 19a, 20, 59] although at higher temperatures, a parallel route to ethene from higher alkene cracking was shown to in-

crease in abundance over H-ZSM-5 zeolite.[21] Together, the results presented in Figures 4 and 5 may suggest that propene is mainly formed from the alkene cycle, whereas ethene is mainly formed from the arene cycle under the conditions used in this study (see Scheme 1). Furthermore, an increase in the predicted catalyst acid strength favors the alkene cycle over the arene cycle.

The end products of hydrogen-transfer reactions, that is, the alkanes, can be analyzed in view of the hydrogen-transfer index (HTI). The HTI for C_2–C_5 products versus conversion over H-MgAlPO-5 and H-SAPO-5 is plotted in Figure 6. The two plots show that the HTI value observed for each individual alkane/alkene pair is higher for H-SAPO-5 than for H-MgAlPO-5. This result links the higher total alkene selectivity observed for the more acidic material of the two, H-MgAPO-5 (see Figure 4a), directly to the relative hydrogen-transfer activity of the two materials. We further note that the HTI is zero for C_3, very low for C_2 (but increasing at decreasing conversion), and substantially higher for C_4 and C_5 over both materials. The difference between C_2, C_4, and C_5 is in line with that reported by Iglesia et al. for H-beta zeolite[60] and reflects the relative stability of primary versus secondary and tertiary carbocation intermediates. The zero HTI value observed for propene, if combined with the non-zero value observed for ethene, is surprising and cannot be explained at this point. However, we note that the same observation is made for both materials.

The mechanism of the hydrogen-transfer reactions in MTH has been scarcely studied, mainly due to the complexity of the product spectrum obtained even at low conversion (e.g. see ref. [30]). Recently, however, studies in which methanol and DME were compared as methylating agents of benzene and isobutene, mainly over H-ZSM-5, yielded new insight into these reactions. Briefly, the studies revealed a key role of methanol and DME as hydrogen-transfer agents between the alkene and arene cycles, as well as between monocyclic arenes and heavier analogues.[31,51] Furthermore, hydrogen-transfer reactions were found to take place at the Brønsted acid sites, whereas isolated Lewis acid sites had negligible activity for both the methylation and hydrogen-transfer reactions.[23] The role of Lewis acid sites in MTH is still not fully revealed. Another recent study of MTH, performed with a H-ZSM-5 catalyst, reported that the rate of methanol conversion correlated with the number of Brønsted acid sites, whereas the aromatics yield correlated with the number of Lewis acid sites in the material.[21] Although the underlying reason for this result is not fully understood, the HTI results obtained suggest that the hydrogen-transfer activity of H-MAPO-5 is less influenced by Brønsted acid strength than other competing reactions in the MTH reaction scheme.

Methane formation from two DME molecules via a methoxy methylene species was recently directly linked to the formation of the first C–C bond in the MTH reaction.[50,61] Whereas such a direct hydrogen transfer between two oxygenate molecules is feasible, the activation energy of this reaction is far higher than that for hydrogen transfer from a DME or methanol molecule to an adjacent alkene molecule.[23,51] Methane formation associated with the MTH initiation reaction is, therefore, assumed to take place mainly in the first part of the reactor, in which the concentration of hydrocarbons is negligible.[62] Another pathway to methane formation is associated with hydrogen transfer from coke precursors to oxygenates, thereby forming polyaromatic molecules. This pathway becomes more abundant with increasing deactivation.[63]

Figure 7 shows the selectivity to methane over the H-MAlPO-5 materials. In general, the selectivity to methane is low over the stronger Brønsted acidic materials, slightly higher over H-SAPO-5, and much higher over H-ZrAPO-5. At low conversion (<15%), the selectivity curves for the medium and strong acid materials converge to a common value. Deeper analysis of the methane formation rates is complicated by the different alkene selectivities over the studied materials. However, we note that the methane selectivity trends are in line with those obtained for the C_{2+} HTI, that is, that materials with low predicted acid strength favor hydrogen-transfer reactions.

Finally, we turn to reactions leading to coke formation and deactivation of the catalysts. Conversion versus time on stream curves for all catalysts are shown in Figure 8, as are the C_4 HTI and C_5 HTI versus aromatics yield plots. Considering first the conversion versus time on stream curves, it is interesting to note that among the materials with high acid strength (i.e. Mg-, Co-, and Zn-substituted AlPO-5), which have very similar effluent product selectivities, the Co- and Zn-substituted materials deactivate much more rapidly than the Mg-containing material. Indeed, upon considering the different WHSVs used in these tests, their DME conversion capacity is comparable to, or lower than, that of H-SAPO-5, which has substantially higher

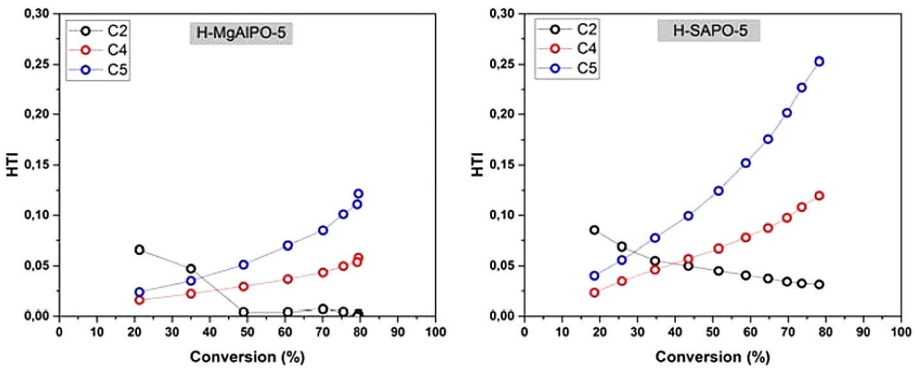

Figure 6. C_2, C_4, and C_5 HTI values for H-MgAlPO-5 and H-SAPO-5 at 450 °C. The HTI for C_3 was zero at all conversion levels and is not included in the figure.

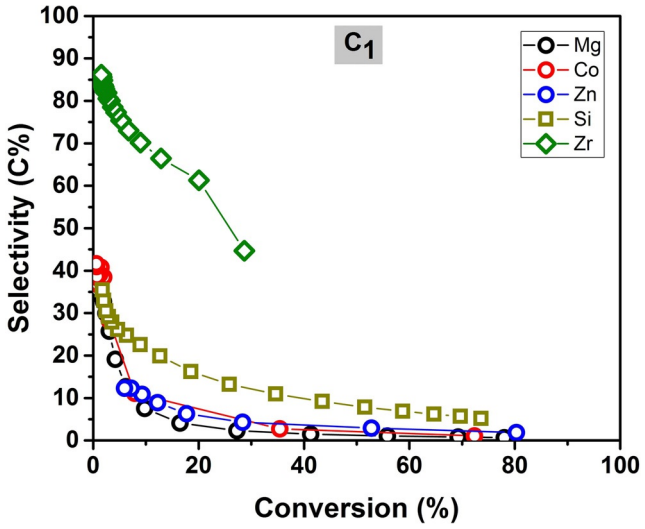

Figure 7. Methane selectivity over the H-MAlPO-5 materials at 450 °C.

activity to hydrogen-transfer products in the effluent than the more acidic materials (Figures 4, 6, and 7). A possible explanation for this result could be leaking of Co and Zn from the H-MAlPO-5 structure during testing. For this reason, in operando X-ray absorption spectroscopy (XAS) measurements were performed for these two materials (Section S9). Briefly, both Co and Zn are in the expected +2 oxidation state after calcination and the +2 oxidation state is retained during activation in air at 550 °C and, more importantly, during catalytic testing mimicking high and low conversion of DME/methanol (see Section S9 for a detailed analysis). With the metal-leaking hypothesis excluded, an alternative explanation was sought. In Figure 8, a clear, positive correlation between HTI and aromatics yield is observed for the Mg- and Si-containing materials, demonstrating that these products are formed by (oxygenate-promoted) hydrogen-transfer reactions. In the Co- and Zn-containing materials, on the other hand, the HTI values are too low to account for the aromatics yield, which suggests another parallel pathway to aromatics formation. Co- and Zn-exchanged zeolites were previously shown to have alkane dehydrogenation activity,[64,65] and we speculate that this is also the case for the isomorphically substituted H-CoAlPO-5 and H-ZnAlPO-5 materials used in this study. Such activity could contribute to more rapid deactivation of the Co- and Zn-containing catalysts.

Overall, the product selectivity data obtained over the isomorphically substituted H-MAPO-5 materials strongly suggest that under the conditions used in this study, an increasing acid strength favors methylation and cracking reactions over hydrogen-transfer reactions. Whereas the detailed interaction between the reactant molecules and the active catalyst is not fully revealed, this study clearly shows that an increasing acid strength enhances the alkene versus arene reaction cycle for total alkene selectivity and also enhances the propene-to-ethene ratio of the H-MAlPO-5 catalysts.

As a final note, the MTH activity trend observed for the materials presented in this study are in line with those previously published by our group for two isostructural zeolite/SAPO pairs, that is, H-SSZ-13 versus H-SAPO-34 (CHA structure) and H-SSZ-24 versus H-SAPO-5 (AFI structure). In those contribu-

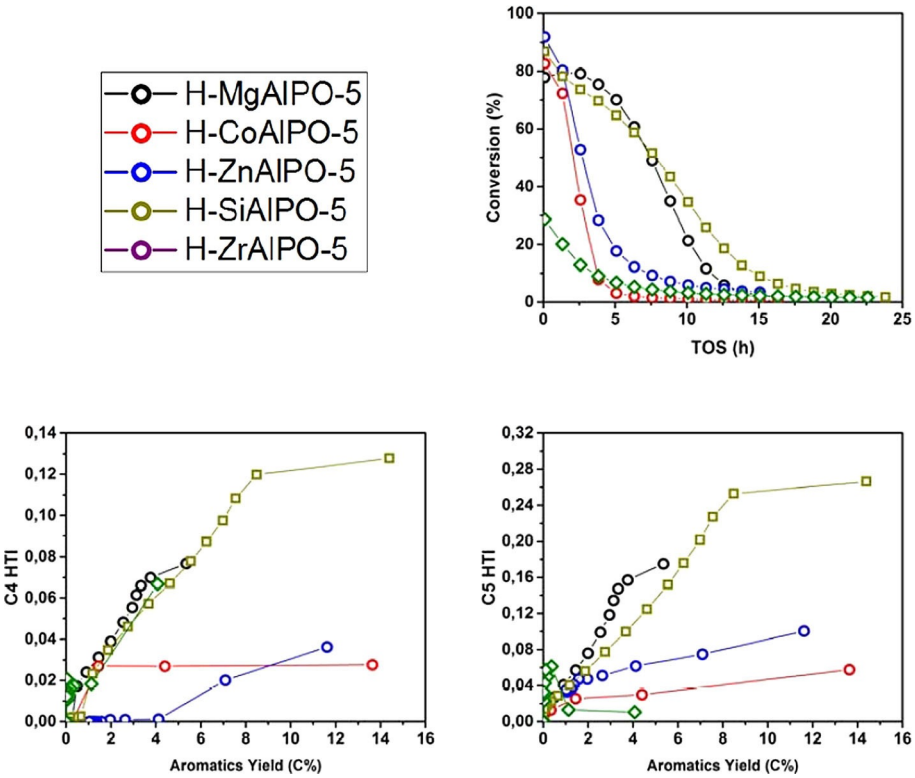

Figure 8. Deactivation plots and C_4/C_5 HTI values versus aromatics yield for DME conversion at 450 °C, p_{DME} = 13 mbar, WHSV = 0.23–1.9 h^{-1}.

tions, the acid strength was assessed experimentally by the relative shift in the O–H stretch frequency of the Brønsted acid site upon CO adsorption, as measured by IR spectroscopy. In both contributions, the material with the highest acid strength, the zeolite, showed substantially higher activity for the MTH reaction than the corresponding SAPO material.[18,66] The product selectivity trends could be reasonably assessed only for the H-SSZ-24 versus H-SAPO-5 pair due to the diffusional restrictions of the H-SSZ-13 versus H-SAPO-34 pair. For H-SSZ-24 versus H-SAPO-5, the selectivity towards ethene and aromatic products was higher for H-SSZ-24 than for H-SAPO-5 upon using methanol as the feed,[18,31] whereas it was similar for the two materials upon using DME as the feed.[31] These results may seem disparate from those presented in the current contribution. However, taking into account the different properties of the material surrounding the active site in the Si–O–Si zeolite lattice, which is more covalently bonded than the Al–O–P MAlPO lattice, these results rather point to a more complex material–performance correlation than previously assessed.

3. Conclusions

Careful design and rigorous execution of the synthesis of a consistent series of isomorphically substituted H-MAlPO-5 materials differing only by the substituted metal and homogenous with respect to the remaining properties allowed us to attribute unambiguously the observed differences in catalytic performance to acid strength associated with modified Brønsted acid sites (BAS). Substantial characterization evidence was provided, firstly showing the homogeneity of the samples with respect to particle size, morphology, surface area, and acid-site density, and secondly strongly indicating the incorporation of the metals as BAS and their stability under the reaction conditions. All materials were shown to be active in the methanol to hydrocarbons (MTH) reaction at 450 °C with clear activity differences, agreeing well with the predicted acid strength.

The materials exhibited clear selectivity differences that could be categorized according to acid strength. Strong acids (Mg, Co, Zn) showed the highest selectivity towards the desired alkene products, with low selectivity towards alkanes and aromatic products. The medium-strength acid (Si) showed increased selectivity towards aromatics and alkanes and a diminished proportion of alkenes. The weakly acidic Zr-substituted material followed the trend of decreasing alkene selectivity with decreasing acid strength.

These encouraging results will be pursued in future studies of individual reactions over the same series of catalysts.

Experimental Section

Catalyst Synthesis

H-MAlPO-5 (M = Mg, Co, Zn) was synthesized hydrothermally from water, triethylamine (Sigma–Aldrich, 99%), orthophosphoric acid (VWR, 85%), Catapal B (Sasol), and $Mg(OAc)_2{\cdot}4H_2O$ or $Co(OAc)_2{\cdot}4H_2O$ or $Zn(OAc)_2{\cdot}4H_2O$ (Sigma–Aldrich, 99.99%). H-ZrAlPO-5 or H-TiAlPO-5 was synthesized from water, triethylamine, orthophosphoric acid (VWR, 85%), Catapal B (Sasol), and titanium(IV) isopropoxide (Sigma–Aldrich, 97%) or zirconium(IV) acetylacetonate (Sigma–Aldrich, 97%), respectively.

For Mg, Co, and Zn, a representative gel composition of $1.0\,Al_2O_3/1.0\,P_2O_5/0.1\,MO/1.0\,Et_3N/50\,H_2O$ was made by stirring Catapal B in 80% of the total added water for 30 min, followed by adding the metal acetate dissolved in the remaining 20% of the water. Orthophosphoric acid was then added dropwise with stirring, followed by the dropwise addition of Et_3N. The solution was stirred for 30 min after the addition of Et_3N and was then crystallized for 4 h at 200 °C in a rotating Teflon-lined steel autoclave. The total weight of the synthesis gel was typically 30 g.

H-ZrAlPO-5 and H-TiAlPO-5 were made by following a similar procedure, with the exception of adding zirconium(IV) acetylacetonate and titanium(IV) isopropoxide directly to the stirring solution of Catapal B and all of the added H_2O without dissolving the metal prior to the addition. AlPO-5 was made following the procedure without adding any metal to the Catapal B and H_2O solution.

The recovered material was washed and centrifuged three times with deionized water and dried at 80 °C for 18 h. Removal of Et_3N was performed by heating the sample to 550 °C at a rate of 1 °C min^{-1} under a 20% O_2 in N_2 atmosphere, followed by calcination at this temperature for 10 h.

Catalyst Characterization

Temperature-programmed desorption of *n*-propylamine was performed at atmospheric pressure in a fixed-bed glass reactor (i.d. 11 mm), similar to the procedure described by Gorte et al.[67] The catalyst powder was pressed and sieved to 250–420 μm and was pretreated in a flow of air at 550 °C. The catalyst was then cooled to 150 °C. N_2 bubbled (80 mL min^{-1}) through a saturator containing *n*-propylamine at room temperature was then fed over the catalyst for 20 min. The excess amount of *n*-propylamine was removed by flowing N_2 at a rate of 80 mL min^{-1} for 4 h at 150 °C. The temperature was then ramped at 20 °C min^{-1} up to 550 °C. The amount of propene desorbed was quantified by using an on-line Pfeiffer Omnistar quadrupole mass spectrometer.

The powder X-ray diffraction (XRD) patterns of the as-synthesized and calcined catalysts were recorded by using a Siemens Bruker D8 Discover instrument with Bragg–Brentano geometry by using CuKα radiation ($\lambda = 1.5406$ Å).

The size and morphology of the zeolite particles were analyzed by scanning electron microscopy (SEM), recorded with a Hitachi SU 8230 FE-SERM. Utilizing energy-dispersive X-ray spectroscopy (EDS) with the same instrument, the elemental composition of the samples was determined.

The BET surface areas and pore volumes were determined by using N_2 physisorption at 77 K by using a Belsorp-mini II instrument. Fresh catalysts were outgassed under vacuum for 4 h, 1 h at 80 °C, followed by a period of 3 h at 300 °C. The BET surface areas were determined on the basis of a linear fit of the data in the relative pressure (p/p_0) range of 0.01 to 0.1.

FTIR spectra were collected by using a Bruker Vertex70 instrument equipped with a liquid-nitrogen-cooled mercury cadmium telluride detector and a Harrick Praying Mantis accessory able to collect data in diffuse reflectance mode (diffuse reflectance infrared Fourier transform, DRIFT). A total of 128 spectra were averaged for each acquisition with a spectral resolution of 2 cm^{-1}. Data are reported in log (R) versus wavenumber. The samples were activated in a

15 mL min^{-1} helium flow from RT to 450 °C (5 °C min^{-1}) to remove water and were then cooled down to 70 °C to dose vapors of deuterated acetonitrile (CD_3CN, supplied by Sigma–Aldrich) as probe molecule, through a 15 mL min^{-1} helium flow. The desorption of the probe was performed by flowing pure helium (under the same conditions) for approximately 15 h. CD_3CN was used instead of CH_3CN to avoid the well-known spectroscopic complication due to Fermi resonance between the ν(CN) vibration and the combination mode δ(CH_3) + ν(CC).

The X-ray absorption spectra at the Co and Zn K-edges were collected in transmission mode at the Swiss–Norwegian Beamline BM31[68,69] of the European Synchrotron Radiation Facility (ESRF). A double-crystal Si(111) monochromator in the continuous scanning mode was used to obtain a monochromatic X-ray beam. Monochromator crystals were detuned to minimize the higher harmonic contribution. A third ionization chamber was used to measure the adsorption of the corresponding metal foil for internal energy calibration.[70] For H-ZnAlPO-5 samples, extended X-ray absorption fine structure (EXAFS) spectra under static conditions were collected up to $k = 15.5$ Å^{-1} in a 15 min acquisition scan, whereas sample activation was monitored by collecting X-ray absorption near-edge structure (XANES) every 3 min. Due to the lower Co content, for H-CoAlPO-5 samples the EXAFS spectra were collected only up to $k = 14.0$ Å^{-1} in a 30 min acquisition scan; XANES spectra were collected in 5 min. Totals of 3 and 5 equivalent EXAFS scans were collected for H-ZnAlPO-5 and H-CoAlPO-5, respectively, and were averaged in k space before the EXAFS data analysis, as described elsewhere.[71]

The measurements were performed in operando mode by using a microtomo reaction cell (hosting the sample in form of self-supported pellet) that allowed sample temperature and gas flows to be remotely controlled and that allowed the gas outlet to be analyzed by a Pfeiffer Omnistar mass spectrometer.[72–74] For H-CoAlPO-5 and H-ZnAlPO-5, the following protocol was followed: 1) sample activation by heating from RT to 550 °C in air (5 °C min^{-1}), monitored by XANES; 2) subsequent cooling in He flow to 450 °C (EXAFS collection); 3) the reaction gas feed (2 mL min^{-1} helium sent through a saturator containing MeOH at room temperature) was sent directly through the microtomo cell (hereafter named 1st cycle) (EXAFS collection after stabilization, monitored by online MS); 4) He was flushed at 450 °C for 2 h; 5) the reaction gas feed (CH_3OH + He) was then sent to a reactor loaded with a commercial zeolite H-ZSM-5 sample (ZeoChem, Si/Al = 59) to convert methanol into hydrocarbons, which subsequently was sent to the sample cell to mimic high conversion over the samples (2nd cycle). Also, for step 5 the EXAFS collection started after stabilization, monitored by online MS.

Catalytic Testing

Catalytic tests were performed at atmospheric pressure in fixed-bed quartz reactors with the catalyst powder pressed and sieved to 250–420 μm. The inner diameter of the reactor was 8 mm. Reaction temperature was monitored by a thermocouple protected by a 3 mm wide quartz sleeve inserted into the middle of the catalyst bed. Dimethyl ether (Praxair or AGA, 25 mol% DME/argon 6.0) was used as the reactant. A range of space velocities was obtained by simultaneously adjusting the flow of the reactant line and a second gas line with pure helium. The catalysts were activated with an initial heating ramp 5 °C min^{-1} under 20% O_2 in helium to 550 °C, and the temperature was kept for 1 h under 100% O_2. Then, the catalysts were cooled to reaction temperature at 5 °C min^{-1} under helium flow.

The catalysts were tested in two sets of experiments. In the first experimental regime for determining DME conversion activity at 450 °C, ≈40 mg of the catalyst was used under a total flow of reactants and inert gas at 50 mL min^{-1} with $p_{DME} = 13$ mbar. This gave a space velocity of 1.9 h^{-1}. In the second experimental regime, to obtain comparable selectivity data at 450 °C, catalyst mass was varied under a fixed total flow reactant and inert gas of 50 mL min^{-1} and $p_{DME} = 13$ mbar. This gave space velocities of 1.9 (H-MgAlPO-5), 1.1 (H-CoAlPO-5), 0.8 (H-ZnAlPO-5), 0.47 (H-SAPO-5), 0.23 (H-ZrAlPO-5), 0.70 (H-TiAlPO-5), and 0.25 $g_{DME}\, g_{cat}^{-1}\, h^{-1}$ (AlPO-5).

The effluent from the reactor was analyzed after 5 min of reaction, and subsequently, every 75 min, by an on-line GC–MS instrument (Agilent 7890 with flame ionization detector and 5975C MS detector) by using two Restek Rtx-DHA-150 columns. Hydrogen (Praxair, purity 6.0) was used as the carrier gas.

Acknowledgements

The authors would like to thank Maria Mykland for synthesis of the AlPO-5 sample and Mustafa Kømurcu, Reynald Henry, and Michael Dyballa for assistance during XAS measurements at the Swiss–Norwegian beamline at ESRF. Kirill A. Lomachenko and Aram L. Bugaev are acknowledged for fruitful discussion on the XAS data. The ESRF is acknowledged for granting beamtime at BM01. M.M., L.M., A.L., and U.O. acknowledge the Norwegian Research Council for financial support through contract 239193. I.A.P. and C.L. acknowledge the Mega-grant of the Russian Federation Government to support scientific research at the Southern Federal University, No. 14.Y26.31.0001.

Keywords: acidity · aluminophosphates · Brønsted acids · hydrocarbons · zeotypes

[1] Y. Tao, H. Kanoh, L. Abrams, K. Kaneko, *Chem. Rev.* **2006**, *106*, 896–910.
[2] K. Egeblad, C. H. Christensen, M. Kustova, C. H. Christensen, *Chem. Mater.* **2008**, *20*, 946–960.
[3] M. Choi, K. Na, J. Kim, Y. Sakamoto, O. Terasaki, R. Ryoo, *Nature* **2009**, *461*, 246–249.
[4] Y. Seo, S. Lee, C. Jo, R. Ryoo, *J. Am. Chem. Soc.* **2013**, *135*, 8806–8809.
[5] E. M. Flanigen, B. M. Lok, R. L. Patton, S. T. Wilson, *Stud. Surf. Sci. Catal.* **1986**, *28*, 103–112.
[6] J. Li, A. Corma, J. Yu, *Chem. Soc. Rev.* **2015**, *44*, 7112–7127.
[7] W. J. Roth, P. Nachtigall, R. E. Morris, P. S. Wheatley, V. R. Seymour, S. E. Ashbrook, P. Chlubná, L. Grajciar, M. Položij, A. Zukal, O. Shvets, J. Čejka, *Nat. Chem.* **2013**, *5*, 628–633.
[8] A. Corma, *J. Catal.* **2003**, *216*, 298–312.
[9] M. E. Davis, *Nature* **2002**, *417*, 813–821.
[10] J. K. Nørskov, T. Bligaard, *Angew. Chem. Int. Ed.* **2013**, *52*, 776–777; *Angew. Chem.* **2013**, *125*, 806–807.
[11] J. Greeley, T. F. Jaramillo, J. Bonde, I. Chorkendorff, J. K. Nørskov, *Nat. Mater.* **2006**, *5*, 909–913.
[12] F. Studt, I. Sharafutdinov, F. Abild-Pedersen, C. F. Elkjær, J. S. Hummelshøj, S. Dahl, I. Chorkendorff, J. K. Nørskov, *Nat. Chem.* **2014**, *6*, 320–324.
[13] U. Olsbye, S. Svelle, M. Bjørgen, P. Beato, T. V. W. Janssens, F. Joensen, S. Bordiga, K. P. Lillerud, *Angew. Chem. Int. Ed.* **2012**, *51*, 5810–5831; *Angew. Chem.* **2012**, *124*, 5910–5933.
[14] M. Stöcker, *Microporous Mesoporous Mater.* **1999**, *29*, 3–48.
[15] I. M. Dahl, S. Kolboe, *Catal. Lett.* **1993**, *20*, 329–336.

[16] I. M. Dahl, S. Kolboe, *J. Catal.* **1994**, *149*, 458 – 464.
[17] I. M. Dahl, S. Kolboe, *J. Catal.* **1996**, *161*, 304 – 309.
[18] M. Westgård Erichsen, S. Svelle, U. Olsbye, *Catal. Today* **2013**, *215*, 216 – 223.
[19] a) S. Svelle, F. Joensen, J. Nerlov, U. Olsbye, K. P. Lillerud, S. Kolboe, M. Bjørgen, *J. Am. Chem. Soc.* **2006**, *128*, 14770 – 14771; b) M. Bjørgen, S. Svelle, F. Joensen, J. Nerlov, S. Kolboe, F. Bonino, L. Palumbo, S. Bordiga, U. Olsbye, *J. Catal.* **2007**, *249*, 195 – 207.
[20] S. Ilias, A. Bhan, *ACS Catal.* **2012**, *3*, 18 – 31.
[21] S. Müller, Y. Liu, F. M. Kirchberger, M. Tonigold, M. Sanchez-Sanchez, J. A. Lercher, *J. Am. Chem. Soc.* **2016**, *138*, 15994 – 16003.
[22] X. Sun, S. Mueller, Y. Liu, H. Shi, G. L. Haller, M. Sanchez-Sanchez, A. C. van Veen, J. A. Lercher, *J. Catal.* **2014**, *317*, 185 – 197.
[23] J. S. Martínez-Espín, K. De Wispelaere, T. V. W. Janssens, S. Svelle, K. P. Lillerud, P. Beato, V. Van Speybroeck, U. Olsbye, *ACS Catal.* **2017**, *7*, 5773 – 5780.
[24] W. E. Farneth, R. J. Gorte, *Chem. Rev.* **1995**, *95*, 615 – 635.
[25] J. Védrine, *Res. Chem. Intermed.* **2015**, *41*, 9387 – 9423.
[26] J. Macht, R. T. Carr, E. Iglesia, *J. Catal.* **2009**, *264*, 54 – 66.
[27] R. T. Carr, M. Neurock, E. Iglesia, *J. Catal.* **2011**, *278*, 78 – 93.
[28] C.-M. Wang, R. Y. Brogaard, B. M. Weckhuysen, J. K. Nørskov, F. Studt, *J. Phys. Chem. Lett.* **2014**, *5*, 1516 – 1521.
[29] R. Y. Brogaard, C.-M. Wang, F. Studt, *ACS Catal.* **2014**, *4*, 4504 – 4509.
[30] M. Westgård Erichsen, K. De Wispelaere, K. Hemelsoet, S. L. C. Moors, T. Deconinck, M. Waroquier, S. Svelle, V. Van Speybroeck, U. Olsbye, *J. Catal.* **2015**, *328*, 186 – 196.
[31] J. S. Martinez-Espin, M. Morten, T. V. W. Janssens, S. Svelle, P. Beato, U. Olsbye, *Catal. Sci. Technol.* **2017**, *7*, 2700.
[32] C.-M. Wang, R. Y. Brogaard, Z.-K. Xie, F. Studt, *Catal. Sci. Technol.* **2015**, *5*, 2814 – 2820 .
[33] S. T. Wilson, B. M. Lok, C. A. Messina, T. R. Cannan, E. M. Flanigen, *J. Am. Chem. Soc.* **1982**, *104*, 1146 – 1147.
[34] H. O. Pastore, S. Coluccia, L. Marchese, *Annu. Rev. Mater. Res.* **2005**, *35*, 351 – 395.
[35] B. M. Weckhuysen, R. R. Rao, J. A. Martens, R. A. Schoonheydt, *Eur. J. Inorg. Chem.* **1999**, 565 – 577.
[36] M. Hartmann, L. Kevan, *Chem. Rev.* **1999**, *99*, 635 – 664.
[37] G. Lischke, B. Parlitz, U. Lohse, E. Schreier, R. Fricke, *Appl. Catal. A* **1998**, *166*, 351 – 361.
[38] S. K. Saha, S. B. Waghmode, H. Maekawa, K. Komura, Y. Kubota, Y. Sugi, Y. Oumi, T. Sano, *Microporous Mesoporous Mater.* **2005**, *81*, 289 – 303.
[39] S. K. Saha, H. Maekawa, S. B. Waghmode, S. A. R. Mulla, K. Komura, Y. Kubota, Y. Sugi, S. J. Cho, *Mater. Trans.* **2005**, *46*, 2659 – 2667.
[40] L. Feng, X. Qi, J. Li, Y. Zhu, L. Zhu, *React. Kinet. Catal. Lett.* **2009**, *98*, 327 – 339.
[41] M. K. Dongare, D. P. Sabde, R. A. Shaikh, K. R. Kamble, S. G. Hegde, *Catal. Today* **1999**, *49*, 267 – 276.
[42] M. Westgård Erichsen, S. Svelle, U. Olsbye, *J. Catal.* **2013**, *298*, 94 – 101.
[43] S. H. Newland, W. Sinkler, T. Mezza, S. R. Bare, R. Raja, *Proc. R. Soc. A* **2016**, *472*, 20160095.
[44] F. Corà, C. R. A. Catlow, *J. Phys. Chem. B* **2001**, *105*, 10278 – 10281.
[45] G. Müller, J. Bódis, G. Eder-Mirth, J. Kornatowski, J. A. Lercher, *J. Mol. Struct.* **1997**, *410*, 173 – 178.
[46] J. Chen, J. M. Thomas, G. Sankar, *J. Chem. Soc., Faraday Trans.* **1994**, *90*, 3455 – 3459.
[47] J. Janchen, M. P. J. Peeters, J. H. M. C. van Wolput, J. P. Wolthuizen, J. H. C. van Hooff, U. Lohse, *J. Chem. Soc., Faraday Trans.* **1994**, *90*, 1033 – 1039.
[48] I. Kustanovich, D. Goldfarb, *J. Phys. Chem.* **1991**, *95*, 8818 – 8823.
[49] M. Popova, C. Minchev, V. Kanazirev, *React. Kinet. Catal. Lett.* **1998**, *63*, 379 – 384.
[50] Z. Wei, Y.-Y. Chen, J. Li, P. Wang, B. Jing, Y. He, M. Dong, H. Jiao, Z. Qin, J. Wang, W. Fan, *Catal. Sci. Technol.* **2016**, *6*, 5526 – 5533.
[51] J. S. Martinez-Espin, K. De Wispelaere, M. Westgård Erichsen, S. Svelle, T. V. W. Janssens, V. Van Speybroeck, P. Beato, U. Olsbye, *J. Catal.* **2017**, *349*, 136 – 148.
[52] W. Dai, W. Kong, G. Wu, N. Li, L. Li, N. Guan, *Catal. Commun.* **2011**, *12*, 535 – 538.
[53] S. Teketel, M. W. Erichsen, F. L. Bleken, S. Svelle, K. P. Lillerud, U. Olsbye in *Catalysis: Vol. 26* (Ed.: J. Spivey, Y.-F. Han, K. M. Dooley), Royal Society of Chemistry, Cambridge, **2014**, pp. 179 – 217.
[54] D. M. McCann, D. Lesthaeghe, P. W. Kletnieks, D. R. Guenther, M. J. Hayman, V. Van Speybroeck, M. Waroquier, J. F. Haw, *Angew. Chem. Int. Ed.* **2008**, *47*, 5179 – 5182; *Angew. Chem.* **2008**, *120*, 5257 – 5260.
[55] M. Westgård Erichsen, M. Mortén, S. Svelle, O. Sekiguchi, E. Uggerud, U. Olsbye, *ChemCatChem* **2015**, *7*, 4143 – 4147.
[56] L. Lin, C. Qiu, Z. Zhuo, D. Zhang, S. Zhao, H. Wu, Y. Liu, M. He, *J. Catal.* **2014**, *309*, 136 – 145.
[57] L. F. Lin, S. F. Zhao, D. W. Zhang, H. Fan, Y. M. Liu, M. Y. He, *ACS Catal.* **2015**, *5*, 4048 – 4059.
[58] J. Meusinger, H. Vinek, J. A. Lercher, *J. Mol. Catal.* **1994**, *87*, 263 – 273.
[59] Y. V. Kissin, *Catal. Rev.* **2001**, *43*, 85 – 146.
[60] D. A. Simonetti, J. H. Ahn, E. Iglesia, *J. Catal.* **2011**, *277*, 173 – 195.
[61] Y. Liu, S. Müller, D. Berger, J. Jelic, K. Reuter, M. Tonigold, M. Sanchez-Sanchez, J. A. Lercher, *Angew. Chem. Int. Ed.* **2016**, *55*, 5723 – 5726; *Angew. Chem.* **2016**, *128*, 5817 – 5820.
[62] S. Müller, Y. Liu, M. Vishnuvarthan, X. Sun, A. C. van Veen, G. L. Haller, M. Sanchez-Sanchez, J. A. Lercher, *J. Catal.* **2015**, *325*, 48 – 59.
[63] H. Schulz, *Catal. Today* **2010**, *154*, 183 – 194.
[64] R. Bulánek, K. Novoveská, B. Wichterlová, *Appl. Catal. A* **2002**, *235*, 181 – 191.
[65] C. O. Arean, M. R. Delgado, P. Nachtigall, H. V. Thang, M. Rubes, R. Bulanek, P. Chlubna-Eliasova, *Phys. Chem. Chem. Phys.* **2014**, *16*, 10129 – 10141.
[66] F. Bleken, M. Bjørgen, L. Palumbo, S. Bordiga, S. Svelle, K.-P. Lillerud, U. Olsbye, *Top Catal.* **2009**, *52*, 218 – 228.
[67] O. Kresnawahjuesa, R. J. Gorte, D. de Oliveira, L. Y. Lau, *Catal. Lett.* **2002**, *82*, 155 – 160.
[68] W. van Beek, O. V. Safonova, G. Wiker, H. Emerich, *Phase Transitions* **2011**, *84*, 726 – 732.
[69] P. M. Abdala, O. V. Safonova, G. Wiker, W. van Beek, H. Emerich, J. A. van Bokhoven, J. Sá, J. Szlachetko, M. Nachtegaal, *Chimia* **2012**, *66*, 699 – 705.
[70] S. Bordiga, E. Groppo, G. Agostini, J. A. van Bokhoven, C. Lamberti, *Chem. Rev.* **2013**, *113*, 1736 – 1850.
[71] C. Lamberti, S. Bordiga, D. Arduino, A. Zecchina, F. Geobaldo, G. Spanó, F. Genoni, G. Petrini, A. Carati, F. Villain, G. Vlaic, *J. Phys. Chem. B* **1998**, *102*, 6382 – 6390.
[72] T. V. W. Janssens, H. Falsig, L. F. Lundegaard, P. N. R. Vennestrøm, S. B. Rasmussen, P. G. Moses, F. Giordanino, E. Borfecchia, K. A. Lomachenko, C. Lamberti, S. Bordiga, A. Godiksen, S. Mossin, P. Beato, *ACS Catal.* **2015**, *5*, 2832 – 2845.
[73] K. A. Lomachenko, E. Borfecchia, C. Negri, G. Berlier, C. Lamberti, P. Beato, H. Falsig, S. Bordiga, *J. Am. Chem. Soc.* **2016**, *138*, 12025 – 12028.
[74] Y. Tulchinsky, C. H. Hendon, K. A. Lomachenko, E. Borfecchia, B. C. Melot, M. R. Hudson, J. D. Tarver, M. D. Korzyński, A. W. Stubbs, J. J. Kagan, C. Lamberti, C. M. Brown, M. Dincă, *J. Am. Chem. Soc.* **2017**, *139*, 5992 – 5997.
[75] A. Miyaki, Y. Sakamoto, Y. Iwase, T. Yashima, R. Koide, K. Motokura, T. Baba, *J. Catal.*, **2013**, *302*, 101 – 114.

Manuscript received: September 20, 2017
Revised manuscript received: October 24, 2017
Version of record online: December 18, 2017

